Collaboration between NDH and KEA3 Allows Maximally Efficient Photosynthesis after a Long Dark Adaptation[1][OPEN]

Leonardo Basso,[a] Wataru Yamori,[b] Ildiko Szabo,[c] and Toshiharu Shikanai[a,2,3]

[a]Department of Botany, Graduate School of Science, Kyoto University, Kyoto 606–8502 Japan
[b]Institute for Sustainable Agro-Ecosystem Services, Graduate School of Agriculture and Life Science, University of Tokyo, Tokyo 188–0002 Japan
[c]Department of Biology, University of Padova, 606–8502 Padova, Italy

ORCID IDs: 0000-0003-3565-9553 (L.B.); 0000-0001-7215-4736 (W.Y.); 0000-0002-3637-3947 (I.S.); 0000-0002-6154-4728 (T.S.)

In angiosperms, the NADH dehydrogenase-like (NDH) complex mediates cyclic electron transport around PSI (CET). K^+ Efflux Antiporter3 (KEA3) is a putative thylakoid H^+/K^+ antiporter and allows an increase in membrane potential at the expense of the ΔpH component of the proton motive force. In this study, we discovered that the *chlororespiratory reduction2-1* (*crr2-1*) mutation, which abolished NDH-dependent CET, enhanced the *kea3-1* mutant phenotypes in Arabidopsis (*Arabidopsis thaliana*). The NDH complex pumps protons during CET, further enhancing ΔpH, but its physiological function has not been fully clarified. The observed effect only took place upon exposure to light of 110 μmol photons m^{-2} s^{-1} after overnight dark adaptation. We propose two distinct modes of NDH action. In the initial phase, within 1 min after the onset of actinic light, the NDH-dependent CET engages with KEA3 to enhance electron transport efficiency. In the subsequent phase, in which the ΔpH-dependent down-regulation of the electron transport is relaxed, the NDH complex engages with KEA3 to relax the large ΔpH formed during the initial phase. We observed a similar impact of the *crr2-1* mutation in the genetic background of the *PROTON GRADIENT REGULATION5* overexpression line, in which the size of ΔpH was enhanced. When photosynthesis was induced at 300 μmol photons m^{-2} s^{-1}, the contribution of KEA3 was negligible in the initial phase and the ΔpH-dependent down-regulation was not relaxed in the second phase. In the *crr2-1 kea3-1* double mutant, the induction of CO_2 fixation was delayed after overnight dark adaptation.

Photosynthesis consists of two sets of reactions, the light reactions and the Calvin-Benson cycle. It takes place in the chloroplast and fixes CO_2 into organic compounds using solar energy. In the light reactions, the absorption of photons activates electron transport in two photosystems. In linear electron transport (LET), PSII catalyzes the light-dependent oxidation of water, resulting in the release of oxygen and protons (H^+) in the thylakoid lumen. The water-derived excised electrons are transferred to PSI through the cytochrome (Cyt) b_6f complex and ultimately to $NADP^+$, producing NADPH. This electron transport is coupled with the translocation of H^+ from the stroma to the thylakoid lumen via the quinone cycle at the Cyt b_6f complex, resulting in the formation of a proton concentration gradient across the thylakoid membrane. This ΔpH contributes to the formation of proton motive force (pmf) in addition to the membrane potential formed across the thylakoid membrane ($\Delta\psi$) that results from the uneven distribution of ions across the membrane. The pmf energizes ATP synthesis via F_oF_1-ATP synthase in chloroplasts (Kramer et al., 2003; Soga et al., 2017) and thus influences the efficiency of the light reactions.

The Calvin-Benson cycle depends on NADPH and ATP produced by the light reactions. To fix a molecule of CO_2 into a carbohydrate, three molecules of ATP and two molecules of NADPH are needed. However, this ratio of ATP to NADPH (1.5) is not satisfied by LET (Shikanai, 2007). Photorespiration, which takes place due to the low specificity of Rubisco, the CO_2-fixing enzyme for CO_2, increases the energetic requirements in terms of ATP, raising the above ratio to 1.67. The additional ATP is thought to be supplied by cyclic electron transport around PSI (CET; Yamori and Shikanai, 2016). In contrast to LET, CET is driven solely by PSI and

[1]This work was supported by the Japanese Society for the Promotion of Science (grant nos. 16H06553 and 19H00992 to T.S.) and the Human Frontier Science Program (grant no. RGP–0052–2015 to T.S. and I.S.).

[2]Author for contact: shikanai@pmg.bot.kyoto-u.ac.jp.
[3]Senior author.
The author responsible for distribution of materials integral to the findings presented in this article in accordance with the policy described in the Instructions for Authors (www.plantphysiol.org) is: Toshiharu Shikanai (shikanai@pmg.bot.kyoto-u.ac.jp).

L.B., I.S., and T.S. designed the research; L.B. performed experiments; W.Y. assisted in the gas-exchange analysis; L.B. and W.Y. analyzed data; all authors wrote the article.

[OPEN]Articles can be viewed without a subscription.
www.plantphysiol.org/cgi/doi/10.1104/pp.20.01069

does not contribute to the net production of reducing power. CET recycles electrons from ferredoxin (Fd) to the plastoquinone (PQ) pool and contributes to the additional generation of ΔpH via the quinone cycle. As a result, CET balances the production ratio of ATP and NADPH. In angiosperms, CET has been proposed to consist of two pathways: the PROTON GRADIENT REGULATION5 (PGR5)/PGR5-like Photosynthetic Phenotype1 (PGRL1) protein-dependent, antimycin A-sensitive pathway and the NADH dehydrogenase-like (NDH) complex-dependent antimycin A-insensitive pathway (Munekage et al., 2004). The NDH complex pumps four protons, coupled with the movement of two electrons, from Fd to PQ, further increasing the efficiency of ΔpH formation (Strand et al., 2017).

In addition to ATP synthesis, the ΔpH component of pmf also contributes to the down-regulation of electron transport (Shikanai, 2014). Acidification of the thylakoid lumen triggers the thermal dissipation of excessively absorbed light energy from the PSII antennae, a process that is monitored by nonphotochemical quenching (NPQ) of chlorophyll fluorescence (Müller et al., 2001). Low lumenal pH also down-regulates the activity of the Cyt b_6f complex, slowing down the rate of electron transport toward PSI (Stiehl and Witt, 1969). CET-dependent ΔpH formation is also necessary to induce the down-regulation of electron transport, as indicated by the phenotype of the *pgr5* mutant. The Arabidopsis (*Arabidopsis thaliana*) *pgr5* mutant cannot induce thermal dissipation under excessive light conditions (Munekage et al., 2002), suggesting that CET-generated ΔpH plays an important role in providing a sufficiently acidic lumen pH that can trigger NPQ. The *pgr5* mutant is also defective in the down-regulation of Cyt b_6f activity, resulting in hypersensitivity of PSI to fluctuating light intensity (Tikkanen et al., 2010). Compared with the physiological function of the PGR5/PGRL1-dependent CET, the contribution of the NDH-dependent CET to photoprotection is somewhat minor, although clear phenotypes have been observed in these mutants at low light intensities and fluctuating light levels (Ueda et al., 2012; Yamori et al., 2015, 2016). Furthermore, the physiological function of the NDH complex has not been fully clarified.

Both ΔpH and $\Delta\psi$ contribute to pmf, but only ΔpH down-regulates electron transport. To optimize the operation of the accelerator (ATP synthesis) and the brake on electron transport, it is necessary to precisely regulate the ratio of the two pmf components as well as the total size of pmf (Cruz et al., 2001; Kramer et al., 2003). Several channels and antiporters localized to the thylakoid membrane regulate the partitioning of the pmf components (Spetea et al., 2017). K^+ Efflux Antiporter3 (KEA3) is thought to be an H^+/K^+ antiporter localized to the thylakoid membrane (Armbruster et al., 2014; Kunz et al., 2014), although its antiport activity has not been experimentally demonstrated (Tsujii et al., 2019). Based on its structure, topology, and the mutant phenotypes, KEA3 most likely moves H^+ from the thylakoid lumen while taking up K^+ as a counter ion. Consequently, KEA3 transforms ΔpH to $\Delta\psi$ and is necessary to rapidly relax the down-regulation of electron transport by raising the luminal pH (i.e. by alkalinizing the lumen). The C-terminal domain of KEA3, KTN (K^+ transport/nucleotide binding), is exposed to the stroma (Wang et al., 2017) and is thought to regulate its activity by monitoring ATP or NADPH levels (Schlosser et al., 1993; Roosild et al., 2002). However, information on the regulation of KEA3 is limited. Armbruster et al. (2014) demonstrated that KEA3 contributes to efficient photosynthesis under fluctuating light conditions. The *disturbed proton gradient regulation* is a dominant mutant allele of *KEA3*, and its mutant phenotype is evident after a long period of dark adaptation (overnight; Wang et al., 2017). KEA3 is likely important during the induction of photosynthesis as well as under fluctuating light intensities. The similarity between the two conditions suggests that KEA3 is required for readjusting the ΔpH-dependent regulation immediately after any drastic change in light conditions.

In this study, we characterized double mutants defective in the CET pathways and KEA3 to understand whether and how the synergy between CET and KEA3 in the regulatory network of photosynthesis affects this process. We focused on the contribution of NDH-dependent CET during the induction of photosynthesis after overnight dark adaptation in the *kea3-1* mutant context. Based on our results, we propose a novel physiological function of the NDH complex: that of allowing flexibility of the regulatory network during the induction of photosynthesis.

RESULTS

The *kea3-1 pgr5-1* Double Mutant Combines the Phenotypes of the Single Mutants in NPQ Induction

To study the collaboration between KEA3 and CET during the induction of photosynthesis, we characterized a series of Arabidopsis mutants. The *pgr5* mutant is defective in the main pathway of CET (Munekage et al., 2002). In this study, we used the original strong allele of *pgr5*, which is referred to as *pgr5-1* in recent studies (Nakano et al., 2019; Yamamoto and Shikanai, 2019). The *kea3-1* mutant is a knockout allele of *KEA3* that encodes a putative H^+/K^+ transporter (Ferro et al., 2010; Armbruster et al., 2014; Kunz et al., 2014). The H^+ efflux activity is important in regulating the lumenal pH and consequently in inducing rapid relaxation of the energy-dependent quenching. In the mutant, the ablation of this pathway leads to a higher NPQ level and a delay in its relaxation (Armbruster et al., 2014).

In this study, we analyzed the *kea3-1 pgr5-1* double mutant. The plants were adapted to the dark overnight (>8 h) before the analysis of electron transport. The Calvin-Benson cycle enzymes are inactivated during this long dark adaptation (Buchanan, 2016). In the *kea3-1* mutant, the relaxation of NPQ was significantly delayed during the induction of photosynthesis by

relatively low light (110 μmol photons m^{-2} s^{-1}) after the overnight dark adaptation, in accordance with our previous data (Fig. 1A; Wang et al., 2017). Since the induction of the Calvin-Benson cycle is delayed to a higher extent after overnight dark adaptation, the contribution of KEA3 to the relaxation of NPQ is higher than after 30 min of dark adaptation.

In wild-type plants, NPQ was transiently induced to the maximum level within 1 min after the onset of actinic light (AL; Fig. 1A). In the *pgr5-1* mutant, AL did not induce this transient peak of NPQ, and the low level of NPQ was not relaxed for 5 min (Supplemental Table S1A). Consistent with previous reports (Armbruster et al., 2014; Wang et al., 2017), the *kea3-1* mutant displayed a slightly higher maximum NPQ level and a delay in the relaxation of NPQ compared with wild-type plants (Fig. 1A). The *kea3-1 pgr5-1* double mutant did not induce a transient peak in NPQ but the NPQ level was higher than that of the *pgr5-1* mutant 1 to 4 min after the onset of AL, and it was higher than that of the *kea3-1* mutant 3 min after the onset of AL (Fig. 1A). This phenotype recorded in the double mutants is consistent with the fact that the *pgr5* mutant and the *kea3-1* mutant are respectively defective in pmf formation and relaxation of ΔpH. We also monitored the induction of LET by a Y(II) parameter representing the quantum yield of PSII after overnight dark adaptation (Fig. 1B). In the *pgr5-1* mutant background, the induction of LET was delayed (Supplemental Table S1A) but Y(II) was close to the wild-type level after 5 min. The *kea3-1* mutation did not affect Y(II) in either the wild-type or the *pgr5-1* mutant context.

The *crr2-1* Mutation Boosts the High NPQ Phenotype of the *kea3-1* Mutant during Induction of Photosynthesis after Overnight Dark Adaptation

Subsequently, we analyzed the collaboration of KEA3 with another pathway of PSI CET depending on the chloroplast NDH complex (Peltier et al., 2016). The *chlororespiratory reduction2-1* (*crr2-1*) mutant is defective in the expression of the *ndhB* gene in chloroplasts and consequently lacks NDH activity (Hashimoto et al., 2003). In contrast to the *pgr5* mutant, the *crr2-1* mutation induced transient NPQ but its peak and relaxation were slightly delayed after overnight dark adaptation (Fig. 1C). The relaxation of NPQ was again more significantly delayed in the *kea3-1* mutant, as confirmed by the Dunnett test (Supplemental Table S1B). Unexpectedly, the induction of NPQ was synergistically enhanced in the *crr2-1 kea3-1* double mutant (Supplemental Table S1B). This is in contrast to the combined, intermediate phenotype of the

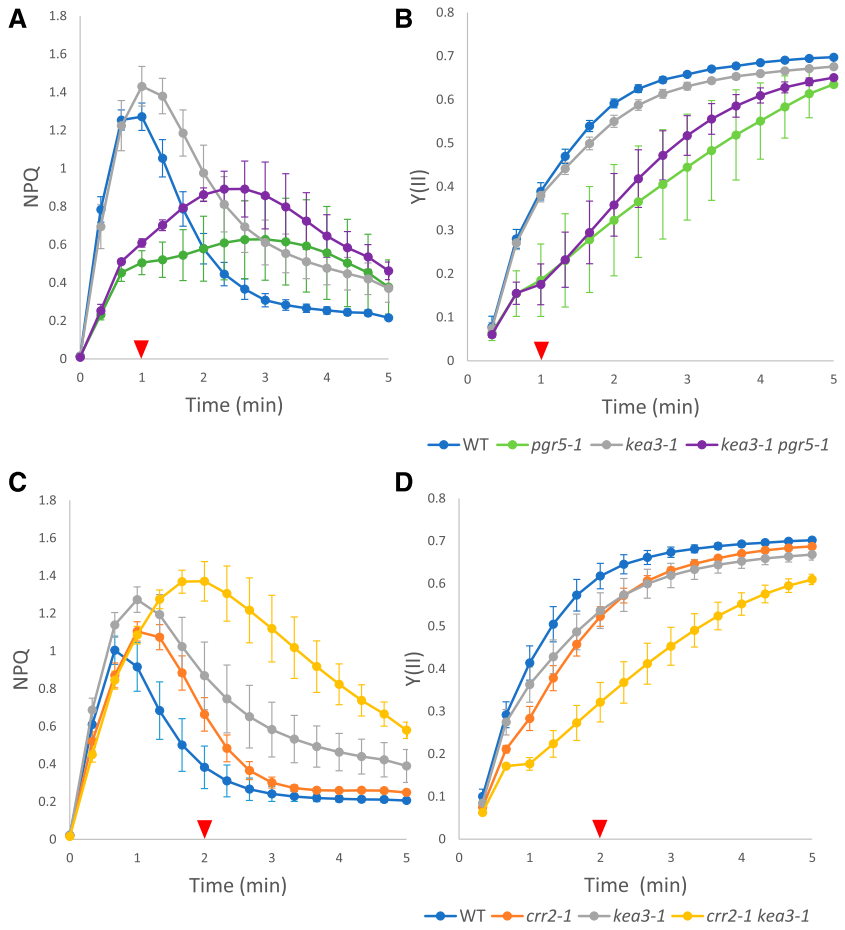

Figure 1. Induction of photosynthesis by non-saturating light (110 μmol photons m^{-2} s^{-1}). Induction and relaxation of NPQ (A and C) and induction of Y(II) (B and D) were measured by chlorophyll fluorescence. Genotypes including *kea3-1* and *pgr5-1* (A and B) and *crr2-1* and *kea3-1* (C and D) were analyzed. Data are shown as means ± SE (n = 4–5). Detached leaves from dark-adapted plants were exposed to AL. Triangles indicate the time points for statistical analyses summarized in Supplemental Table S1. WT, Wild type.

pgr5-1 kea3-1 double mutant (Fig. 1A). Interestingly, it took longer for transient NPQ to peak in the *crr2-1 kea3-1* double mutant (100–120 s after the onset of AL) than in the wild-type (40 s after the onset of AL).

In the *crr2-1* and *kea3-1* single mutants, LET monitored by Y(II) was only mildly affected during the induction of photosynthesis after overnight dark adaptation. However, the induction of LET was delayed in the *crr2-1 kea3-1* double mutant (Fig. 1D; Supplemental Table S1B). Taken together with the observations of NPQ induction and relaxation (Fig. 1C), our interpretation is that the thylakoid lumen may have been more acidified in the *crr2-1 kea3-1* double mutant than in the single mutants. This proposition is consistent with the idea that the *kea3-1* mutant context accumulates more protons in the lumen, but it is unclear how the defect in the NDH complex enhances the *kea3-1* phenotype. We therefore focused on this phenotype of the double mutant to analyze the collaboration between KEA3 and NDH.

To assess the impact of the long overnight dark adaptation on the *crr2-1 kea3-1* mutant phenotype, we analyzed the induction of photosynthesis at the same photosynthetic photon flux density (PPFD; 110 μmol photons m^{-2} s^{-1}) after a 30-min dark adaptation (Fig. 2). This short dark adaptation is routinely used before chlorophyll fluorescence analysis to relax pmf formed under growth lighting. Both single mutants (*crr2-1* and *kea3-1*) showed similar induction and relaxation curves of NPQ to those after overnight dark adaptation (Figs. 1C and 2A). However, NPQ was not further affected in the *crr2-1 kea3-1* double mutant and was similar to that of the *kea3-1* single mutant (Supplemental Table S2). Thus, the overnight dark adaptation enhanced the phenotype of the *crr2-1 kea3-1* mutant. A similar trend was also observed in Y(II), although the induction of LET was also delayed in the *crr2-1 kea3-1* double mutant with respect to other genotypes after the 30-min dark adaptation (Fig. 2B; Supplemental Table S2).

The *crr2-1* mutant is defective in a pentatricopeptide repeat protein required for the expression of the plastid *ndhB* gene (Hashimoto et al., 2003). The *crr2-1* mutation might also affect the expression of other plastid gene(s), and the phenotype of the *crr2-1 kea3-1* double mutant might be caused by the altered expression of the unknown gene(s) rather than *ndhB*. To eliminate this possibility, we also created the double mutant of *kea3-1* with the *photosynthetic ndh subunit 2 of subcomplex b* (*pnsb2*) mutant defective in the nuclear gene encoding a subunit of the NDH complex (Ifuku et al., 2011). As with the *crr2-1* mutation, the *pnsb2* mutation enhanced the mutant phenotype of *kea3-1* in NPQ and Y(II), although the difference was not statistically significant by the Tukey-Kramer test (Supplemental Fig. S1, A and B; Supplemental Table S3). We confirmed that the defects in the accumulation of the NDH complex enhanced the *kea3-1* mutant phenotype after overnight dark adaptation.

Collaboration of the NDH Complex with KEA3 Is Necessary to Efficiently Induce LET

By monitoring the change in absorbance of the PSI reaction center chlorophylls (P700), we analyzed the status of PSI photochemistry during the induction of photosynthesis at 110 μmol photons m^{-2} s^{-1}. Y(I) is often used to estimate the quantum yield of PSI and is calculated from a ratio of P700 in a reduced state; it is not limited by the acceptor side (P700 functioning in electron transport). The Y(ND) parameter is calculated as the ratio of oxidized P700 ($P700^+$) per total P700 and represents the nonphotochemical energy dissipation from oxidized PSI. Y(ND) is used to estimate the operation of the ΔpH-dependent down-regulation of the Cyt b_6f complex (photosynthetic control), which is important to control the rate of electron transport toward PSI (Yamamoto and Shikanai, 2019). In contrast, Y(NA) represents the fraction of reduced P700 that cannot be oxidized by a saturation pulse due to the lack of acceptors (nonphotochemical energy dissipation from reduced PSI). In addition to the actual shortage of electron acceptors from PSI, Y(NA) is induced when excess electrons accumulate on the donor side of PSI (Klughammer and Schreiber, 1994). The induction of Y(NA) is related to the photodamage of PSI and inevitably occurs during the very early induction of photosynthesis

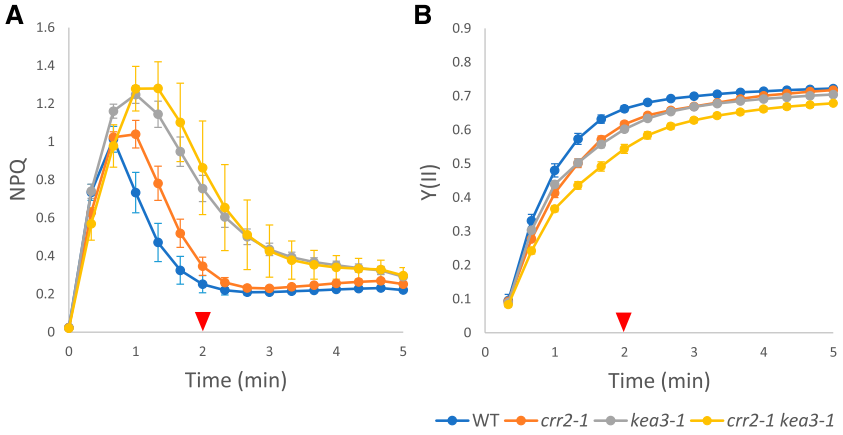

Figure 2. Induction of photosynthesis by nonsaturating light (110 μmol photons m^{-2} s^{-1}) after a 30-min dark adaptation. Induction and relaxation of NPQ (A) and induction of Y(II) (B) were measured by chlorophyll fluorescence in a set of genotypes including *crr2-1* and *kea3-1*. Data are shown as means ± SE (n = 4–5). Detached leaves from dark-adapted plants were exposed to AL. Triangles indicate the time points for statistical analyses summarized in Supplemental Table S2. WT, Wild type.

and also just after the shift from low light to high light, even in wild-type plants (Yamamoto et al., 2016). Because light energy absorbed by the PSI antennae is photochemically used or nonphotochemically dissipated via one of three processes, the sum of Y(I), Y(ND), and Y(NA) is 1.

After a 30-min dark adaptation, no difference was observed in PSI photochemistry among wild-type, *crr2-1*, *kea3-1*, and *crr2-1 kea3-1* plants (Supplemental Fig. S2). Y(ND) was transiently induced during the early induction of the Calvin-Benson cycle but was immediately substituted by Y(I). The time course of the induction and relaxation of Y(ND) was similar to that of NPQ (Fig. 2), suggesting a transient acidification of the thylakoid lumen. Y(NA) was only induced during the initial phase (<40 s) but was immediately relaxed by the induction of Y(I) and Y(ND).

After overnight dark adaptation, the induction of Y(I) and Y(ND) was slightly delayed in the *crr2-1* mutant compared with the wild type (Fig. 3, A and B; Supplemental Table S4). Y(ND) peaked at 60 s after the onset of AL in wild-type plants, but it peaked at 80 to 100 s in the *crr2-1* mutant (Fig. 3B). Consequently, it took longer to relax Y(NA) (Fig. 3C). The contribution of Y(ND) was slightly higher in the *kea3-1* mutant than in the wild type during the subsequent relaxation and steady-state phases. The *kea3-1* mutant behaved almost like the *crr2-1* mutant. In the *crr2-1 kea3-1* double mutant, however, the *crr2-1* phenotypes were amplified (Fig. 3). The induction of Y(I) and Y(ND) was significantly delayed. The peak of Y(ND) was observed at 140 to 160 s after the onset of AL, resulting in the delay in the relaxation of Y(NA). During the relaxation and steady-state phases, the level of Y(ND) was higher than that in the other genotypes, resulting in a lower Y(I) level (Fig. 3B). This phenotype is consistent with the higher maximum level of NPQ and its delay in relaxation and the reduced level of Y(II) in the *crr2-1 kea3-1* double mutant (Fig. 1, C and D). During the relaxation and steady-state phases (more than 1 min after the onset of AL in wild-type plants), the thylakoid lumen was likely more acidified in the *crr2-1 kea3-1* double mutant than in other genotypes. Taken together with the results of chlorophyll fluorescence analyses (Fig. 1, C and D), we propose that the NDH complex likely contributes to the rapid acidification of the thylakoid lumen during the initial phase of photosynthetic induction (less than 60 s after the onset of AL) after overnight dark adaptation. On the other hand, the collaboration of the NDH complex with KEA3 is required for relaxing the ΔpH in the next relaxation phase (60–180 s after the onset of AL). This phase is important to efficiently induce photosynthesis, as can be deduced by the delayed induction of Y(II) and Y(I) (LET) in the *crr2-1 kea3-1* double mutant. A similar trend was observed in the *kea3-1 pnsb2* double mutant (Supplemental Fig. S1, C–E).

To confirm our hypothesis that NDH contributes to the initial lumenal acidification, we performed electrochromic shift (ECS) experiments. The ECS signal represents the changes in the absorption of photosynthetic pigments (mainly carotenoids), peaking at 515 to 520 nm, in the presence of an electric field across the thylakoid membrane (Klughammer et al., 2013). To characterize the phenotype of the *crr2-1 kea3-1* double mutant more comprehensively, we analyzed the ECS signal during the induction of photosynthesis at 110 μmol photons m^{-2} s^{-1}

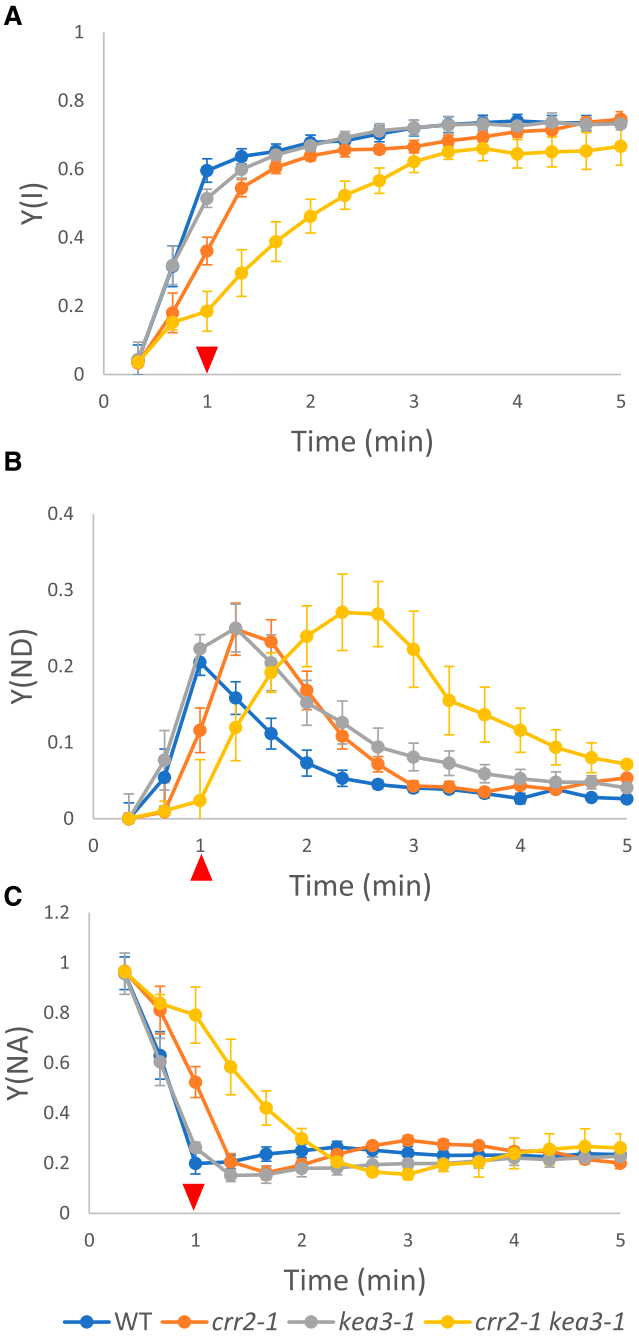

Figure 3. Induction of photosynthesis by nonsaturating light (110 μmol photons m^{-2} s^{-1}) was monitored by P700 parameters after overnight dark adaptation. Y(I) (A), Y(ND) (B), and Y(NA) (C) were analyzed. Data are shown as means ± SE (n = 4–5). Detached leaves from dark-adapted plants were exposed to AL. Triangles indicate the time points for statistical analyses summarized in Supplemental Table S4. WT, Wild type.

(Fig. 4). The total amplitude of ECS changes (ECS_t) from a dark pulse during AL illumination (110 μmol photons m^{-2} s^{-1}) represents the total size of pmf formed in the light (Bailleul et al., 2010). The ECS_t level was standardized by the ECS signal triggered with a single turnover flash (ECS_{ST}) to compensate for the effects of the differences in leaf thickness and the content of reaction centers. In the wild-type plants, the size of pmf peaked at 40 s after the onset of AL after both conditions of dark adaptation and was followed by relaxation (Fig. 4, A and C). This is consistent with the course of induction and relaxation of NPQ and Y(ND) in the wild-type plants (Figs. 1C and 3B). For 1 min after the onset of AL, the size of pmf was smaller in the *crr2-1 kea3-1* double mutant than that of other genotypes after overnight dark adaptation (Fig. 4A; Supplemental Table S5). This is consistent with the slower induction of Y(ND) seen in the double mutant (Fig. 3B) and suggests that the NDH-dependent CET is probably important to induce a transient increase in ΔpH in the initial phase (<60 s). The size of pmf did not show any peaks during the induction of photosynthesis in the *crr2-1 kea3-1* double mutant, and the level was similar to that of the other genotypes at 2 min after the onset of AL (Fig. 4A). The size of pmf does not simply explain the delayed peak and relaxation of NPQ and Y(ND) in the *crr2-1 kea3-1* double mutant (Figs. 1C and 3B). It is necessary to consider relative partitioning (i.e. the higher contribution of ΔpH to pmf in the double mutant).

The g_{H^+} parameter, which is considered to represent the proton conductivity of ATP synthase (Kramer et al., 2004; Kohzuma et al., 2013), was determined by chasing the initial fast relaxation kinetics of the ECS in the dark. The g_{H^+} was drastically reduced in the *crr2-1 kea3-1* double mutant after overnight dark adaptation (Fig. 4B; Supplemental Table S5), suggesting a delay in the activation of ATP synthase. After the 30-min dark adaptation, the reduction in g_{H^+} was milder in the *crr2-1 kea3-1* double mutant and similar to that in the *kea3-1* mutant, although a mild reduction was observed also in the *crr2-1* mutant context (Fig. 4D; Supplemental Table S5).

The thioredoxin-dependent redox modification of the γ-subunit of ATP synthase regulates the activity of ATP synthase during the induction of photosynthesis. The reduced form of the γ-subunit was modified with 4-acetoamido-4-maleimidylstilbene-2,2-disulfonate (AMS) and was separated from the oxidized form by nonreducing SDS-PAGE (Motohashi et al., 2001). Immediately after the onset of AL (30 s), the γ-subunit was reduced to the steady-state level, and no difference was observed in the reduction state of the γ-subunit between the wild type and the *crr2-1 kea3-1* mutant after a 30-min or overnight dark adaptation (Supplemental Fig. S3). Thus, the activation of the γ-subunit does not explain the lower g_{H^+} in the *crr2-1 kea3-1* double mutant.

The Contribution of KEA3 Is Negligible to Induce Photosynthesis Efficiently under High Light after Overnight Dark Adaptation

For studying the photosynthetic induction after overnight dark adaptation, we selected a relatively low PPFD of 110 μmol photons m^{-2} s^{-1} because the phenotype of the *kea3-1* mutant was most clearly observed at that PPFD (Wang et al., 2017). We also tested the induction of electron transport at a higher PPFD (300 μmol

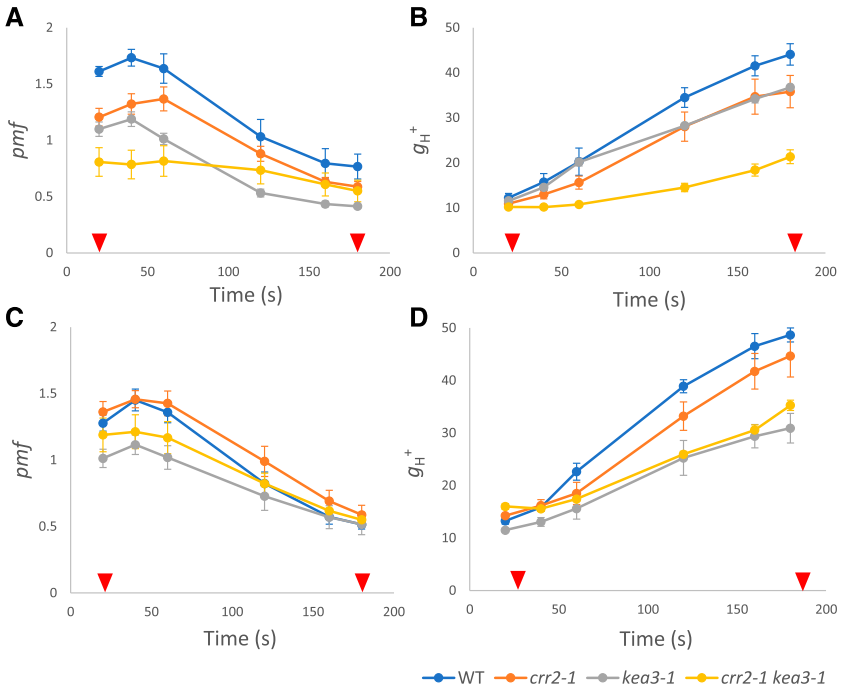

Figure 4. ECS analysis of a set of genotypes including *crr2-1* and *kea3-1*. Photosynthesis was induced by nonsaturating light (110 μmol photons m^{-2} s^{-1}) after overnight dark adaptation (A and B) and a 30-min dark adaptation (C and D). The size of light-induced pmf (ECS_t/ECS_{ST}; A and C) and g_{H^+} (B and D) were determined. Data are shown as means ± SE (n = 4–5). Detached leaves from dark-adapted plants were exposed to AL. Triangles indicate the time points for statistical analyses summarized in Supplemental Table S5. WT, Wild type.

photons m^{-2} s^{-1}) after overnight dark adaptation (Fig. 5). Compared with the induction at 110 μmol photons m^{-2} s^{-1}, a higher level of NPQ was induced and was not relaxed for 280 s in the light in wild-type and *kea3-1* plants (Fig. 5A). The induction of NPQ was slightly delayed in the *crr2-1* mutant, the phenotype that was enhanced in the *crr2-1 kea3-1* double mutant. At 3 min after the onset of AL, the levels of NPQ became similar among all the genotypes. Induction of Y(II) was mildly affected in the *crr2-1* mutant background before 120 s and in the *kea3-1* mutant background after 120 s (Fig. 5B). Induction of Y(I) was more significantly delayed than Y(II) in the *crr2-1* mutant background (*crr2-1* and *crr2-1 kea3-1*) at 80 s after the onset of AL, but Y(I) was restored to the wild-type level at 120 s (Fig. 5C; Supplemental Table S6). This delay in Y(I) may reflect the lack of the NDH-dependent CET, since Y(II) was only mildly affected in the *crr2-1* mutant background. The delay in the NPQ induction may be explained by the absence of NDH-dependent CET (Fig. 5, A–C). Consistent with this idea, the induction of Y(ND) was severely delayed at 80 s after the onset of AL in the *crr2-1* mutant background. This was reflected by the delay in the relaxation of Y(NA) at the same time (Fig. 5, D and E; Supplemental Table S6). Notably, similar phenotypes were observed between the *crr2-1* mutant and the *crr2-1 kea3-1* double mutant, in contrast to the synergistic effect observed at 110 μmol photons m^{-2} s^{-1} (Figs. 1, 3, and 5). The function of KEA3 and also probably the reverse action of NDH are likely necessary only at a relatively low light intensity, where the ΔpH-dependent down-regulation is immediately relaxed. At a higher PPFD of 300 μmol photons m^{-2} s^{-1}, however, the ΔpH-dependent down-regulation is not relaxed once it is induced.

The mutant phenotypes were not observed after the 30-min dark adaptation (Fig. 2). Subsequently, we analyzed how long dark adaptation is necessary for monitoring the contribution of NDH and KEA3 during the induction of photosynthesis at 110 μmol photons m^{-2} s^{-1} (Supplemental Fig. S4). As the representative mutant phenotypes of the *crr2-1 kea3-1* double mutant, we selected high NPQ and Y(ND) and low Y(II) levels at 2 min after the onset of AL after overnight dark adaptation (Figs. 1, C and D, and B3B). After a 1-h dark adaptation, the *crr2-1 kea3-1* mutant did not show any phenotypes, as after a 30-min dark adaptation (Fig. 2; Supplemental Fig. S4). However, a similar phenotype to the overnight dark adaptation was detected after a 2- to 3-h dark adaptation. At least 2 h of dark adaptation is necessary to induce the state in which the collaboration

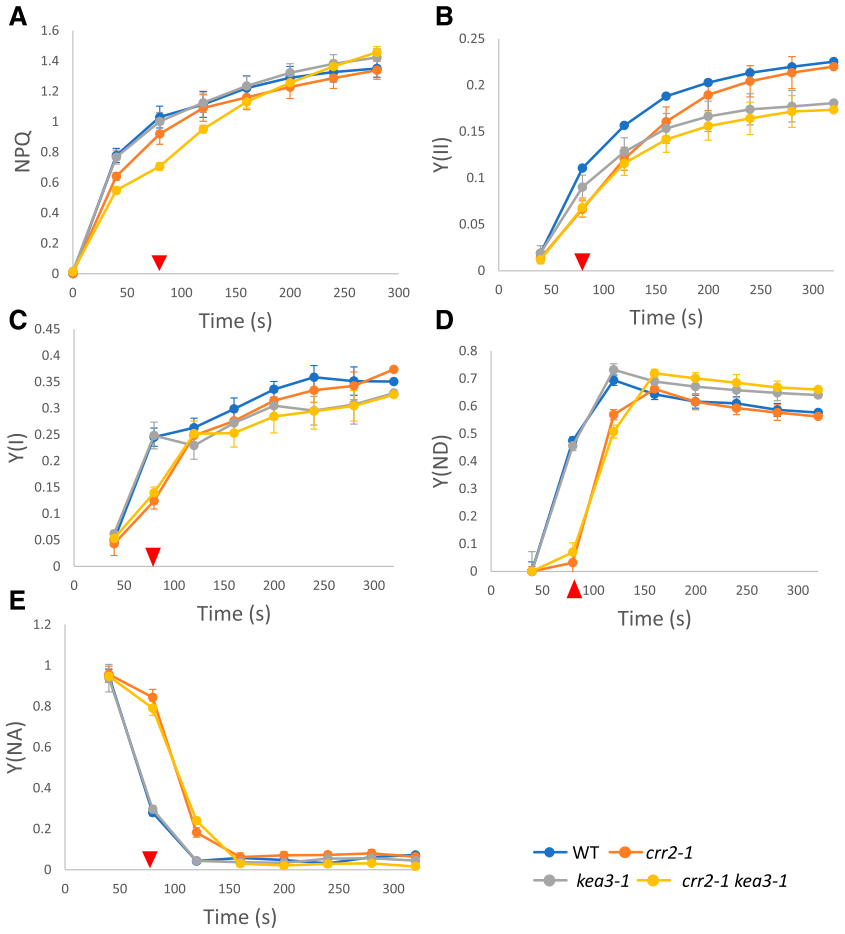

Figure 5. Induction of photosynthesis by relatively high light (300 μmol photons m^{-2} s^{-1}) after overnight dark adaptation. Induction and relaxation of NPQ (A) and induction of Y(II) (B) were measured by chlorophyll fluorescence in a set of genotypes including *crr2-1* and *kea3-1*. Y(I) (C), Y(ND) (D), and Y(NA) (E) were also analyzed by monitoring the P700 absorbance changes. Data are shown as means ± SE ($n = 5$). Detached leaves from dark-adapted plants were exposed to AL. Triangles indicate the time points for statistical analyses summarized in Supplemental Table S6. WT, Wild type.

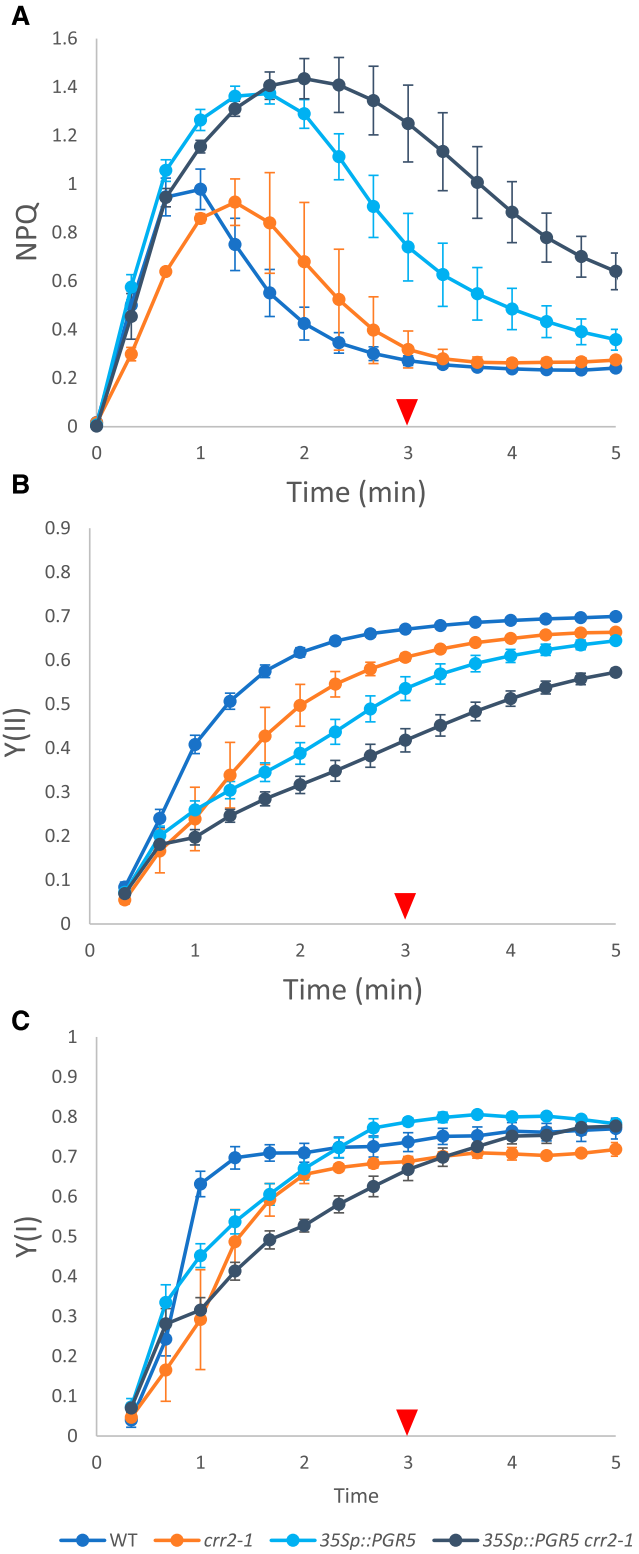

Figure 6. Induction of photosynthesis by nonsaturating light (110 μmol photons m^{-2} s^{-1}) after overnight dark adaptation was analyzed in *crr2-1* and *35Sp::PGR5* genotypes. Induction and relaxation of NPQ (A) and induction of Y(II) (B) and Y(I) (C) were measured by chlorophyll fluorescence (A and B) and P700 absorbance change (C) analyses. Data are shown as means ± SE (n = 4–5). Detached leaves from dark-adapted plants were exposed to AL. Triangles indicate the time points for statistical analyses summarized in Supplemental Table S7. WT, Wild type.

of the NDH complex and KEA3 is necessary to induce photosynthesis efficiently.

The *crr2-1* Mutation Also Enhanced the Phenotypes of the *35Sp::PGR5* Line

As shown above, the *crr2-1* mutation boosted the phenotypes due to the high ΔpH in the *kea3-1* mutant, especially after the overnight dark adaptation (Figs. 1 and 3–5). We tested the impact of the *crr2-1* mutation in another genetic context that exhibited a high-ΔpH phenotype (Fig. 6). Expressing the *35Sp::PGR5* transgene accumulates high levels of the PGR5 protein and conditionally activates the PGR5-dependent CET when the stroma is highly reduced, as it is during the induction of photosynthesis (Okegawa et al., 2007). We therefore generated a line with the transgene inserted into the same genome position in the *crr2-1* mutant background by crossing the *PGR5*-overexpressing line with the *crr2-1* mutant (*35Sp::PGR5 crr2-1*). As in the *kea3-1* mutant, the maximum level of transient NPQ was enhanced and its relaxation was delayed in the *35Sp::PGR5* line after overnight dark adaptation (Fig. 6A; Supplemental Table S7). As in the *kea3-1* mutant background, the phenotype of the *35Sp::PGR5* line in NPQ was enhanced by adding the *crr2-1* mutation. A similar trend was observed in the Y(ND) parameter (Supplemental Fig. S5; Supplemental Table S7), suggesting stronger acidification of the thylakoid lumen. Consistent with this idea, the induction of LET was delayed in the *35Sp::PGR5* line and was further slowed in the *35Sp::PGR5 crr2-1* line (Fig. 6, B and C; Supplemental Table S7). In the same way with the *kea3-1* mutant background, the NDH complex is necessary to relax the transiently formed high ΔpH in the *35Sp::PGR5* background. The NDH complex engages with KEA3 to rapidly relax the transiently induced high ΔpH, a process that is necessary to efficiently induce LET after overnight dark adaptation.

Collaboration of the NDH Complex with KEA3 to Induce Efficient CO_2 Fixation after Overnight Dark Adaptation

The collaboration of the NDH complex with KEA3 is necessary to efficiently induce LET, as evaluated by the chlorophyll fluorescence and spectroscopic analyses (Figs. 1 and 3). Finally, we analyzed the impact of the *crr2-1* and *kea3-1* mutations and the *crr2-1 kea3-1* double mutation on the induction of CO_2 fixation at 110 μmol photons m^{-2} s^{-1} by GFS3000 (Walz), a system for the assessment of plant photosynthesis (CO_2 uptake) or respiration (CO_2 release) and transpiration (Fig. 7). Simultaneously, we monitored the induction of Y(I) and Y(II) by the Dual-PAM system (Supplemental Fig. S6).

After the 30-min dark adaptation, the rate of CO_2 fixation was not affected in any of the genetic backgrounds (Fig. 7B; Supplemental Table S8). Consistently, the induction of Y(I) and Y(II) was unaffected, although it was slightly delayed at 20 s after the onset of AL in the *crr2-1 kea3-1* double mutant (Supplemental Fig. S6, B and D). In contrast, the induction of CO_2 fixation was more evidently delayed in the *crr2-1 kea3-1* double mutant after overnight dark adaptation (Fig. 7A; Supplemental Table S8). A similar phenotype was also observed in the induction of Y(I) and Y(II) (Supplemental Fig. S6, A and C). We conclude that the collaboration of the NDH complex with KEA3 is needed to induce photosynthesis efficiently after the overnight dark adaptation.

DISCUSSION

The ΔpH-dependent regulation of electron transport optimizes photosynthesis, especially under fluctuating light conditions. To regulate the lumenal pH, it is necessary to adjust the size and the component partitioning of pmf (Cruz et al., 2001). In angiosperms, CET plays a central role in the regulation of pmf size (Munekage et al., 2002, 2004; DalCorso et al., 2008; Wang et al., 2015; Yamamoto et al., 2016). The PGR5/PGRL1-dependent CET is essential to induce ΔpH-dependent regulation: the energy-dependent quenching, monitored by NPQ, and the donor-side regulation of PSI at the Cyt b_6f complex monitored by Y(ND) (Munekage et al., 2004; Suorsa et al., 2012). On the other hand, channels and transporters localized to the thylakoid membrane regulate the partitioning of pmf components (Kramer et al., 2003, Spetea et al., 2017). The putative H^+/K^+ antiporter KEA3 was discovered only recently, and little is known about it, especially regarding the regulation of its activity (Armbruster et al., 2014; Kunz et al., 2014; Wang et al., 2017). Furthermore, the link between the two regulatory systems, CET, and the modulation of transthylakoid ion movement remains unclear. In the Arabidopsis *pgr5-1* mutant, the lack of CET results in a reduced size of pmf (Munekage et al., 2002; Wang et al., 2017). The size of pmf was complemented to the wild-type level by the introduction of *Physcomitrella patens* genes encoding Flavodiiron (Flv) proteins into the Arabidopsis *pgr5-1* mutant (Yamamoto et al., 2016). Flv reduces oxygen to water at the acceptor side of PSI (Allahverdiyeva et al., 2015), and the Flv-dependent pseudo-CET (water-water cycle) contributes to pmf formation in place of the PGR5-dependent CET. Despite the increased size of pmf, the contribution of $\Delta\psi$ to pmf was greater in the *pgr5-1* mutant plants accumulating Flv, resulting in the reduced size of NPQ at moderate light intensities (Yamamoto et al., 2016). This observation suggests cross talk between PGR5-dependent CET and the regulation of transthylakoid ion movement to optimize the size and component partitioning of pmf, although the exact molecular mechanism is unclear.

In this study, we analyzed the collaboration between two CET pathways and KEA3. Similar to the *pgr5-1* mutant, the

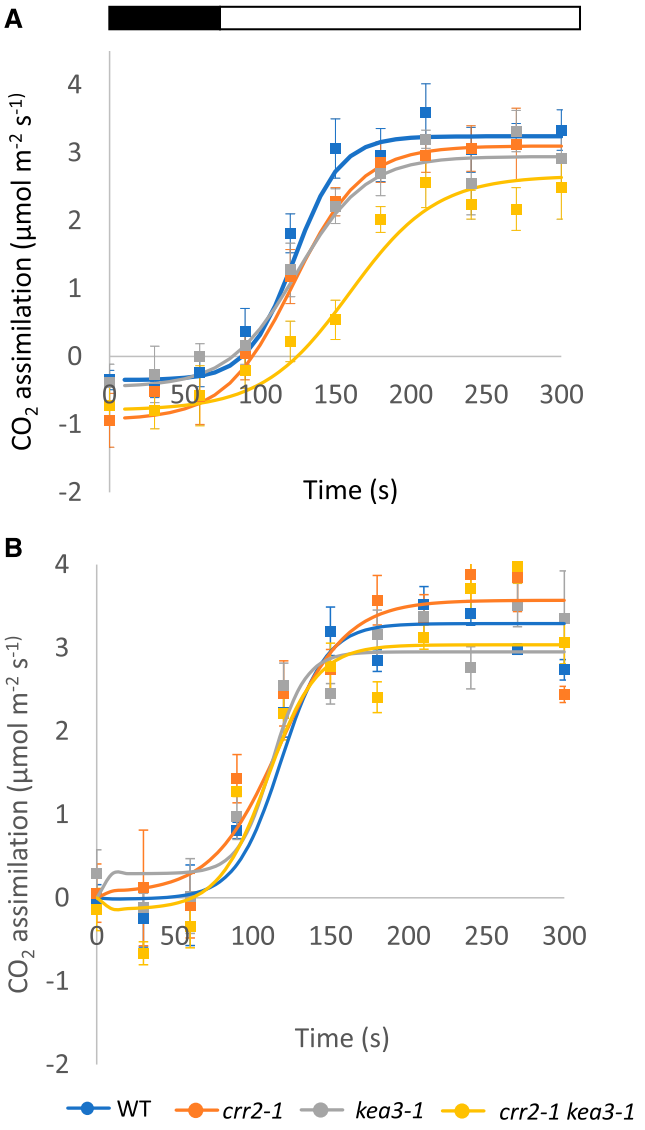

Figure 7. Analysis of CO_2 fixation under nonsaturating light (110 μmol photons m^{-2} s^{-1}). A set of genotypes including *crr2-1* and *kea3-1* was analyzed. Data are shown as means ± SE (n = 4–5). Detached leaves from dark-adapted plants were exposed to AL. The statistical analyses are summarized in Supplemental Figure S8. The black and white bars at top represent the analysis in the dark and the light, respectively. WT, Wild type.

kea3-1 pgr5-1 double mutant did not induce transient NPQ but induced higher NPQ 1 to 5 min after the onset of AL than the *pgr5-1* mutant (Fig. 1A). Both phenotypes are consistent with those of the single mutants. On the other hand, the *crr2-1* and *pndb2* mutations synergistically enhanced the high-NPQ phenotype of the *kea3-1* mutant (Fig. 1C; Supplemental Fig. S1A). The NDH complex is part of the CET machinery, which contributes to pmf formation, so it was not expected that, when defective, it would enhance the high-NPQ phenotype of the *kea3-1* mutant. To explain the phenotypes of the *crr2-1* single mutant and the *crr2-1 kea3-1* double

mutant after overnight dark adaptation (Fig. 1, C and D), we may consider two distinct modes of action of the NDH complex based on the following considerations. (1) During the initial phase of photosynthetic induction (<60 s), the peak in transient NPQ was delayed in the *crr2-1* mutant (Fig. 1C). A similar delay was observed in the induction of Y(ND) (Fig. 3B). It thus seems likely that the NDH-dependent CET is necessary, as well as the PGR5-dependent CET, to efficiently induce the transient NPQ. (2) In the subsequent phase for the relaxation of NPQ (1–5 min after the onset of AL), the NPQ induction was more enhanced in the *crr2-1 kea3-1* double mutant than in the wild type and the single mutants (Fig. 1C). Because this phenotype was not evident in the *crr2-1* single mutant, the NDH complex is dispensable when KEA3 is functional. The *kea3-1* mutant exhibited the high-NPQ phenotype to a lower extent in this phase as well, suggesting that substitution of ΔpH by $\Delta\psi$ is necessary for rapidly relaxing NPQ. A few questions remain unanswered. How does the NDH complex alleviate the *kea3-1* defect in this phase? The NDH complex couples the pumping of H^+ across the thylakoid membrane with electron transport from Fd to PQ (Strand et al., 2017). This CET activity is unlikely to support the antiport function of H^+/K^+ in KEA3. In the presence of a large pmf or ΔpH, the NDH complex may move H^+ backward from the thylakoid lumen. It is possible that this reverse flow of H^+ is coupled with the PQ-dependent Fd reduction. Although direct evidence is still lacking, uncouplers enhanced the NDH-dependent PQ reduction, suggesting that the back pressure of pmf controls NDH activity and may induce a reverse reaction (Strand et al., 2017). The uphill reaction of complex I (PQ-dependent Fd reduction) was also reported in bacteria, including *Rhodobacter capsulatus* (Herter et al., 1998) and *Thiobacillus ferrooxidans* (Elbehti et al., 2000), and was recently suggested in cyanobacteria (Nikkanen et al., 2020).

The two modes of NDH activity were also supported by the analysis of P700 (Fig. 3). Induction of Y(ND) was delayed in the *crr2-1* single mutant and more severely in the *crr2-1 kea3-1* double mutant (Fig. 3B). The delay in the induction of Y(ND) resulted in the delay in the relaxation of Y(NA). Of interest is that the induction of Y(II) and Y(I) was similarly delayed at 40 to 60 s after the onset of AL (Figs. 1D and 3A). This delay in the LET induction may be due to the acceptor limitation from PSI (Fig. 3C), but it is unclear how the synergy between the NDH complex and KEA3 is necessary in the initial phase. To conclude the reverse reaction of the NDH complex, direct biochemical evidence would be necessary. We do not eliminate the possibility that the lack of NDH-dependent CET secondarily disturbs the movement of protons from the thylakoid membrane.

In the second phase for relaxing NPQ, namely 1 to 5 min after the onset of AL, a high level of Y(ND) was induced in the *crr2-1 kea3-1* double mutant, supporting the idea that the thylakoid lumen was unusually acidified. This is probably the reason for the further delay in LET observed in Y(II) and Y(I) (Figs. 1D and 3A). In this phase, we speculate that the reverse reaction of the NDH complex takes place to optimize the lumenal pH, as proposed before. Disturbance of electron transport regulation in both phases likely resulted in the delay observed in the induction of CO_2 fixation (Fig. 7A). The reduced size of g_{H^+} in the *crr2-1 kea3-1* double mutant is consistent with the delay in the induction of CO_2 fixation (Fig. 4B) but was not due to the delay in the reduction of the γ-subunit of ATP synthase (Supplemental Fig. S3).

It is even more challenging to explain the molecular basis of the double mutant phenotypes in the initial phase (<60 s after the onset of AL). The total size of pmf peaked 40 to 60 s after the onset of AL in the wild type and the *crr2-1* and *kea3-1* single mutants (Fig. 4A), consistent with the peaks of NPQ and Y(ND) in these genotypes (Figs. 1C and 3B). Puzzlingly, the size of pmf did not fluctuate and was consistently low during the induction of photosynthesis in the *crr2-1 kea3-1* double mutant (Fig. 4A). To explain the delayed induction and relaxation of NPQ and Y(ND), we need to consider the greater contribution of $\Delta\psi$ to pmf in the initial phase and the more significant contribution of ΔpH to pmf in the second phase. It is not feasible to analyze the partitioning of the pmf components during the induction of photosynthesis because the ECS signal is still unstable. Although we do not understand the mechanism, KEA3 was also required for transiently inducing the high pmf during the initial phase (Fig. 4A). Although the *crr2-1* and *kea3-1* single mutants induced similar levels of transient pmf within 40 s after the onset of AL, Y(ND) induction was affected only in the *crr2-1* mutant (Fig. 3B). Because KEA3 is a putative H^+/K^+ antiporter, it would be logical to consider a higher contribution of ΔpH to pmf in the *kea3-1* mutant context. On the other hand, induction of Y(ND) was delayed at 40 s after the onset of AL in the *crr2-1* single mutant as well as in the *crr2-1 kea3-1* double mutant (Fig. 3B), although the level of pmf in the *crr2-1* mutant was between the levels of the wild type and the *crr2-1 kea3-1* mutant (Fig. 4A). The phenotype may be explained by the threshold of ΔpH required for the induction of Y(ND). It is also possible that the NDH complex may be necessary to induce a transiently higher contribution of ΔpH to pmf in the initial phase.

In contrast to the induction by relatively low PPFD (110 μmol photons m^{-2} s^{-1}), the *kea3-1* mutation did not enhance the *crr2-1* phenotype at 300 μmol photons m^{-2} s^{-2} after overnight dark adaptation (Fig. 5). The lack of the NDH-dependent CET resulted in the delayed induction of Y(I), subsequently delaying the induction of ΔpH-dependent down-regulation of electron transport monitored in NPQ and Y(ND). The contribution of the NDH-dependent CET after long dark adaptation has been also suggested in another study (Nikkanen et al., 2018). This function of NDH is likely the same as that in the initial phase of photosynthetic induction (<60 s) observed at 110 μmol photons m^{-2} s^{-1}. The impact of the *kea3-1* mutation in the *crr2-1* mutant background was not observed at

300 μmol photons m^{-2} s^{-1}. In the subsequent phase (1 to 5 min after the onset of AL), there was no difference anymore in photosynthetic parameters between the wild type and any of the mutants at 300 μmol photons m^{-2} s^{-1} (Fig. 5). This is consistent with the fact that the contribution of KEA3 is not observed at high light intensities (Wang and Shikanai, 2019). The second phase is probably specifically observed at a relatively low light intensity, at which the transiently induced ΔpH-dependent down-regulation is relaxed. In the process, the collaboration of KEA3 and probably the reverse reaction of the NDH complex is necessary.

In conclusion, in this study, we focused on the mutant phenotype observed after overnight dark adaptation. The phenotype was suppressed after 30 min of dark adaptation (Figs. 2 and 4, C and D). Collaboration between the NDH complex and KEA3 is needed to efficiently induce photosynthesis in the initial phase at relatively low light intensity after overnight dark adaptation. This may be related to ion homeostasis in the stroma to activate the Calvin-Benson cycle (Bloom and Lancaster, 2018). Further work is necessary to understand how exactly the two types of machinery interact. However, the idea of regulation of an H^+-conducting complex by an ion channel/transporter in the thylakoids is more than plausible, in light of observations that a calcium-dependent potassium channel has been shown to functionally interact with complex IV of the respiratory chain (Bednarczyk et al., 2013) while complex II is regulated by an ATP-dependent potassium channel (Wojtovich et al., 2013).

MATERIALS AND METHODS

Plant Material and Growth Conditions

Arabidopsis (*Arabidopsis thaliana*) wild-type plants (ecotype Columbia *gl1*), mutant plants, and transgenic plants overexpressing *PGR5* were grown in soil in a growth chamber (50–60 μmol photons m^{-2} s^{-1}) under long-day conditions (16-h-light/8-h-dark cycle, 23°C) for 3 to 4 weeks. For the ECS analysis, plants were cultured under short-day conditions (8-h-light/16-h-dark cycle, 23°C) for 6 to 8 weeks. Fully expanded leaves were used for experiments. The mutants and transgenic lines used in this study are *kea3-1* (GABI_170G09; Wang et al., 2017), *pgr5* (Munekage et al., 2002), *crr2-1* (Hashimoto et al., 2003), *pnsb2/ndf2* (Salk_111363; Takabayashi et al., 2009), and *35Sp::PGR5* (#2; Okegawa et al., 2007).

Analysis of Chlorophyll Fluorescence

Chlorophyll fluorescence and P700 absorption changes in the PSI reaction center were measured simultaneously using a portable chlorophyll fluorometer (Dual-PAM-100 MODULAR version chlorophyll fluorescence and P700 absorption analyzer, equipped with a p700 dual-wavelength emitter at 830 and 870 nm; Walz). Plants were kept in the dark for 30 min or 8 h before the measurements, and detached leaves were used for the analysis. Minimal fluorescence in the dark-adapted state (F_o) was excited by a weak measuring light (620 nm) at a photon flux density of 0.05 to 0.1 μmol photons m^{-2} s^{-1}. A saturating pulse of light (SP; 300 ms, 10,000 μmol photons m^{-2} s^{-1}) was applied to determine the maximal fluorescence in the dark-adapted state (F_m) and during AL illumination (F_m'). The steady-state fluorescence level (F_s) was recorded during AL illumination (110 μmol photons m^{-2} s^{-1}). The maximum quantum yields of PSII and NPQ were calculated as F_v/F_m and $(F_m - F_m')/F_m'$, respectively. Y(II) was calculated as $(F_m - F_s)/F_m'$.

The redox change of P700 was assessed by monitoring the changes in absorbance of transmission light at 830 and 875 nm. Pm was determined by the application of an SP in the presence of far-red light (720 nm). The maximal level of oxidized P700 during AL illumination (Pm′) was determined by the SP application. The P700 signal P was recorded just before an SP. Y(I) was calculated as (Pm′ – P)/Pm. Y(NA) was calculated as (Pm – Pm′)/Pm. Y(ND) was calculated as P/Pm. Three complementary quantum yields were defined: Y(I) + Y(NA) + Y(ND) = 1 (Klughammer and Schreiber, 1994). The relative level of reduced P700 was calculated as 1 – Y(ND). The value can vary between 0 (P700 fully oxidized) and 1 (P700 fully reduced) in a given state.

ECS Measurements

The ECS measurements were carried out using a Walz Dual-PAM-100 equipped with a P515/535 module (Walz). Measurements were carried out in ambient air. Before the measurements, 4- to 5-week-old plants grown under a short-day photoperiod were dark adapted overnight, followed by a 10-min illumination with 110 μmol photons m^{-2} s^{-1} actinic red light. A 1-s dark pulse was applied at the different time points to record ECS_t, which represents the size of the light-induced pmf and was estimated from the total amplitude of the rapid decay of the ECS signal during the dark pulse, as described previously (Wang et al., 2015). ECS_t levels were normalized against the ECS_{ST}, as measured in dark-adapted leaves before recording. This normalization makes it possible to take into account possible changes in leaf thickness and chloroplast density between leaves (Takizawa et al., 2008).

Gas Exchange

The gas-exchange rate was measured using a gas-exchange cuvette (GFS3000; Walz) equipped with a Dual-PAM Cuvette (DUAL 3010 cuvette; Walz) with an illuminated area of 1.3 cm^2 and 1 mm chamber depth. Leaf temperature was kept close to 23°C (22.5°C to 23.5°C). Incoming CO_2 and water concentrations were controlled via the GFS3000 gas-exchange system. The gas stream (400 μmol s^{-1}) passed the leaf twice, over the lower and upper sides, before entering the infrared gas analyzer for assessment of CO_2 uptake and water release at a PPFD of 100 μmol photons m^{-2} s^{-1} under adjusted air conditions (400 μL L^{-1} CO_2, 21% [v/v] oxygen). The rate of mitochondrial respiration in the light was assumed to be equal to that in the dark. The gross rate of CO_2 assimilation was calculated as the sum of the net CO_2 assimilation rate and the dark respiration rate. Measurements were performed on individual 4-week-old seedlings that had been kept in the dark for 30 min or 8 h before the analysis.

SDS-PAGE and Immunoblot Analyses

Plants were frozen in liquid nitrogen after dark adaptation or after a different light treatment and disrupted using a Shake master (Shake Master Neo; bms). Proteins were extracted in SDS sample buffer (2% [w/v] SDS, 62.5 mM Tris-HCl [pH 6.8], 7.5% [v/v] glycerol, and 6 M urea) containing the protease inhibitor cocktail Complete (Roche) and the specific thiol-labeling reagent AMS (Invitrogen). The samples were incubated for 60 min at room temperature to complete the labeling of thiol groups with AMS. Protein concentration was determined via a bicinchoninic acid protein assay (Pierce). Proteins were separated by nonreducing SDS-PAGE using the conventional Laemmli (Tris-Gly) system (Laemmli, 1970) and transferred onto polyvinylidene fluoride membranes using a semidry blotting apparatus. Immunodetection was carried out using specific antibodies. Signals were detected using an ECL Plus Western Blotting Detection Kit (GE Healthcare) and visualized by a LAS300 chemiluminescence analyzer (Fuji Film). Immunoblots were quantified by Imagemaster software (Amersham Pharmacia Biotech).

Statistical Analyses

Statistical analyses were performed using the Tukey-Kramer test and the Dunnett test.

Accession Numbers

The sequence data from this article can be found in The Arabidopsis Information Resource database (https://www.arabidopsis.org/) under the following accession numbers: *crr2* (At3g46790), *kea3* (At4g04850), *pgr5* (At2g05620), and *PnsB2* (At1g64770).

Supplemental Data

The following supplemental materials are available.

Supplemental Figure S1. Induction of photosynthesis under nonsaturating light (110 μmol photons m^{-2} s^{-1}) after overnight dark adaptation.

Supplemental Figure S2. Induction of photosynthesis under nonsaturating light (110 μmol photons m^{-2} s^{-1}) after the 30-min dark adaptation.

Supplemental Figure S3. Photoreduction patterns of the γ-subunit of ATP synthase.

Supplemental Figure S4. Impact of the time of dark adaptation on electron transport.

Supplemental Figure S5. Induction of photosynthesis by nonsaturating light (110 μmol photons m^{-2} s^{-1}) after overnight dark adaptation.

Supplemental Figure S6. Chlorophyll fluorescence and P700 absorbance changes were simultaneously analyzed during the induction of CO_2 fixation.

Supplemental Table S1. Statistical analysis of Figure 1.

Supplemental Table S2. Statistical analysis of Figure 2.

Supplemental Table S3. Statistical analysis of Supplemental Figure S1.

Supplemental Table S4. Statistical analysis of Figure 3.

Supplemental Table S5. Statistical analysis of Figure 4.

Supplemental Table S6. Statistical analysis of Figure 5.

Supplemental Table S7. Statistical analysis of Figure 6 and Supplemental Figure S5, A and B.

Supplemental Table S8. Statistical analysis of Figure 7 and Suppplemental Figure S6.

ACKNOWLEDGMENTS

We thank Dr. Masaru Kono (University of Tokyo) for support with the gas-exchange analysis and Dr. Hiroshi Yamamoto (Kyoto University) for help with the statistical analyses.

Received August 10, 2020; accepted September 16, 2020; published September 25, 2020.

LITERATURE CITED

Allahverdiyeva Y, Isojärvi J, Zhang P, Aro EM (2015) Cyanobacterial oxygenic photosynthesis is protected by flavodiiron proteins. Life (Basel) **5:** 716–743

Armbruster U, Carrillo LR, Venema K, Pavlovic L, Schmidtmann E, Kornfeld A, Jahns P, Berry JA, Kramer DM, Jonikas MC (2014) Ion antiport accelerates photosynthetic acclimation in fluctuating light environments. Nat Commun **5:** 5439

Bailleul B, Cardol P, Breyton C, Finazzi G (2010) Electrochromism: A useful probe to study algal photosynthesis. Photosynth Res **106:** 179–189

Bednarczyk P, Wieckowski MR, Broszkiewicz M, Skowronek K, Siemen D, Szewczyk A (2013) Putative structural and functional coupling of the mitochondrial BK channel to the respiratory chain. PLoS ONE **8:** e68125

Bloom AJ, Lancaster KM (2018) Manganese binding to Rubisco could drive a photorespiratory pathway that increases the energy efficiency of photosynthesis. Nat Plants **4:** 414–422

Buchanan BB (2016) The path to thioredoxin and redox regulation in chloroplasts. Annu Rev Plant Biol **67:** 1–24

Cruz JA, Sacksteder CA, Kanazawa A, Kramer DM (2001) Contribution of electric field ($\Delta\psi$) to steady-state trans thylakoid proton motive force (pmf) in vitro and in vivo: Control of pmf parsing into $\Delta\psi$ and ΔpH by ionic strength. Biochemistry **40:** 1226–1237

DalCorso G, Pesaresi P, Masiero S, Aseeva E, Schünemann D, Finazzi G, Joliot P, Barbato R, Leister D (2008) A complex containing PGRL1 and PGR5 is involved in the switch between linear and cyclic electron flow in Arabidopsis. Cell **132:** 273–285

Elbehti A, Brasseur G, Lemesle-Meunier D (2000) First evidence for existence of an uphill electron transfer through the bc_1 and NADH-Q oxidoreductase complexes of the acidophilic obligate chemolithotrophic ferrous ion-oxidizing bacterium *Thiobacillus ferrooxidans*. J Bacteriol **182:** 3602–3606

Ferro M, Brugiere S, Salvi D, Seigneurin-Berny D, Court M, Moyet L, Ramus C, Miras S, Mellal M, Le Gall S, et al (2010) AT_CHLORO, a comprehensive chloroplast proteome database with subplastidial localization and curated information on envelope proteins. Mol Cell Proteomics **9:** 1063–1084

Hashimoto M, Endo T, Peltier G, Tasaka M, Shikanai T (2003) A nucleus-encoded factor, CRR2, is essential for the expression of chloroplast *ndhB* in Arabidopsis. Plant J **36:** 541–549

Herter SM, Kortlüke CM, Drews G (1998) Complex I of *Rhodobacter capsulatus* and its role in reverted electron transport. Arch Microbiol **169:** 98–105

Ifuku K, Endo T, Shikanai T, Aro EM (2011) Structure of the chloroplast NADH dehydrogenase-like complex: Nomenclature for nuclear-encoded subunits. Plant Cell Physiol **52:** 1560–1568

Klughammer C, Schreiber U (1994) An improved method, using saturating light pulses, for the determination of photosystem I quantum yield via $P700^+$-absorbance changes at 830 nm. Planta **192:** 261–268

Klughammer C, Siebke K, Schreiber U (2013) Continuous ECS-indicated recording of the proton-motive charge flux in leaves. Photosynth Res **117:** 471–487

Kohzuma K, Dal Bosco C, Meurer J, Kramer DM (2013) Light- and metabolism-related regulation of the chloroplast ATP synthase has distinct mechanisms and functions. J Biol Chem **288:** 13156–13163

Kramer DM, Cruz JA, Kanazawa A (2003) Balancing the central roles of the thylakoid proton gradient. Trends Plant Sci **8:** 27–32

Kramer DM, Johnson G, Kiirats O, Edwards GE (2004) New fluorescence parameters for the determination of Q_A redox state and excitation energy fluxes. Photosynth Res **79:** 209–218

Kunz HH, Gierth M, Herdean A, Satoh-Cruz M, Kramer DM, Spetea C, Schroeder JI (2014) Plastidial transporters KEA1, -2, and -3 are essential for chloroplast osmoregulation, integrity, and pH regulation in Arabidopsis. Proc Natl Acad Sci USA **111:** 7480–7485

Laemmli UK (1970) Cleavage of structural proteins during the assembly of the head of bacteriophage T4. Nature **227:** 680–685

Motohashi K, Kondoh A, Stumpp MT, Hisabori T (2001) Comprehensive survey of proteins targeted by chloroplast thioredoxin. Proc Natl Acad Sci USA **98:** 11224–11229

Müller P, Li XP, Niyogi KK (2001) Non-photochemical quenching: A response to excess light energy. Plant Physiol **125:** 1558–1566

Munekage Y, Hashimoto M, Miyake C, Tomizawa K, Endo T, Tasaka M, Shikanai T (2004) Cyclic electron flow around photosystem I is essential for photosynthesis. Nature **429:** 579–582

Munekage Y, Hojo M, Meurer J, Endo T, Tasaka M, Shikanai T (2002) PGR5 is involved in cyclic electron flow around photosystem I and is essential for photoprotection in Arabidopsis. Cell **110:** 361–371

Nakano H, Yamamoto H, Shikanai T (2019) Contribution of NDH-dependent cyclic electron transport around photosystem I to the generation of proton motive force in the weak mutant allele of *pgr5*. Biochim Biophys Acta Bioenerg **1860:** 369–374

Nikkanen L, Santana Sánchez A, Ermakova M, Rögner M, Cournac L, Allahverdiyeva Y (2020) Functional redundancy between flavodiiron proteins and NDH-1 in *Synechocystis* sp. PCC 6803. Plant J **103:** 1460–1476

Nikkanen L, Toivola J, Trotta A, Diaz MG, Tikkanen M, Aro EM, Rintamäki E (2018) Regulation of cyclic electron flow by chloroplast NADPH-dependent thioredoxin system. Plant Direct **2:** e00093

Okegawa Y, Long TA, Iwano M, Takayama S, Kobayashi Y, Covert SF, Shikanai T (2007) A balanced PGR5 level is required for chloroplast development and optimum operation of cyclic electron transport around photosystem I. Plant Cell Physiol **48:** 1462–1471

Peltier G, Aro EM, Shikanai T (2016) NDH-1 and NDH-2 plastoquinone reductases in oxygenic photosynthesis. Annu Rev Plant Biol **67:** 55–80

Roosild TP, Miller S, Booth IR, Choe S (2002) A mechanism of regulating transmembrane potassium flux through a ligand-mediated conformational switch. Cell **109:** 781–791

Schlosser A, Hamann A, Bossemeyer D, Schneider E, Bakker EP (1993) NAD^+ binding to the *Escherichia coli* K^+-uptake protein TrkA and sequence similarity between TrkA and domains of a family of

dehydrogenases suggest a role for NAD^+ in bacterial transport. Mol Microbiol **9:** 533–543

Shikanai T (2007) Cyclic electron transport around photosystem I: Genetic approaches. Annu Rev Plant Biol **58:** 199–217

Shikanai T (2014) Central role of cyclic electron transport around photosystem I in the regulation of photosynthesis. Curr Opin Biotechnol **26:** 25–30

Soga N, Kimura K, Kinosita K Jr., Yoshida M, Suzuki T (2017) Perfect chemomechanical coupling of FoF1-ATP synthase. Proc Natl Acad Sci USA **114:** 4960–4965

Spetea C, Herdean A, Allorent G, Carraretto L, Finazzi G, Szabo I (2017) An update on the regulation of photosynthesis by thylakoid ion channels and transporters in Arabidopsis. Physiol Plant **161:** 16–27

Stiehl HH, Witt HT (1969) Quantitative treatment of the function of plastoquinone in photosynthesis. Z Naturforsch B **24:** 1588–1598

Strand DD, Fisher N, Kramer DM (2017) The higher plant plastid NAD(P)H dehydrogenase-like complex (NDH) is a high efficiency proton pump that increases ATP production by cyclic electron flow. J Biol Chem **292:** 11850–11860

Suorsa M, Järvi S, Grieco M, Nurmi M, Pietrzykowska M, Rantala M, Kangasjärvi S, Paakkarinen V, Tikkanen M, Jansson S, et al (2012) PROTON GRADIENT REGULATION5 is essential for proper acclimation of Arabidopsis photosystem I to naturally and artificially fluctuating light conditions. Plant Cell **24:** 2934–2948

Takabayashi A, Ishikawa N, Obayashi T, Ishida S, Obokata J, Endo T, Sato F (2009) Three novel subunits of Arabidopsis chloroplastic NAD(P)H dehydrogenase identified by bioinformatic and reverse genetic approaches. Plant J **57:** 207–219

Takizawa K, Kanazawa A, Kramer DM (2008) Depletion of stromal P_i induces high "energy-dependent" antenna exciton quenching (q_E) by decreasing proton conductivity at CF_O-CF_1 ATP synthase. Plant Cell Environ **31:** 235–243

Tikkanen M, Grieco M, Kangasjärvi S, Aro EM (2010) Thylakoid protein phosphorylation in higher plant chloroplasts optimizes electron transfer under fluctuating light. Plant Physiol **152:** 723–735

Tsujii M, Kera K, Hamamoto S, Kuromori T, Shikanai T, Uozumi N (2019) Evidence for potassium transport activity of Arabidopsis KEA1-KEA6. Sci Rep **11:** 10040

Ueda M, Kuniyoshi T, Yamamoto H, Sugimoto K, Ishizaki K, Kohchi T, Nishimura Y, Shikanai T (2012) Composition and physiological function of the chloroplast NADH dehydrogenase-like complex in *Marchantia polymorpha*. Plant J **72:** 683–693

Wang C, Shikanai T (2019) Modification of activity of the thylakoid H^+/K^+ antiporter KEA3 disturbs ΔpH-dependent regulation of photosynthesis. Plant Physiol **181:** 762–773

Wang C, Yamamoto H, Narumiya F, Munekage YN, Finazzi G, Szabo I, Shikanai T (2017) Fine-tuned regulation of the K^+/H^+ antiporter KEA3 is required to optimize photosynthesis during induction. Plant J **89:** 540–553

Wang C, Yamamoto H, Shikanai T (2015) Role of cyclic electron transport around photosystem I in regulating proton motive force. Biochim Biophys Acta **1847:** 931–938

Wojtovich AP, Smith CO, Haynes CM, Nehrke KW, Brookes PS (2013) Physiological consequences of complex II inhibition for aging, disease, and the mKATP channel. Biochim Biophys Acta **1827:** 598–611

Yamamoto H, Shikanai T (2019) PGR5-dependent cyclic electron flow protects photosystem I under fluctuating light at donor and acceptor sides. Plant Physiol **179:** 588–600

Yamamoto H, Takahashi S, Badger MR, Shikanai T (2016) Artificial remodeling of alternative electron flow by flavodiiron proteins in Arabidopsis. Nat Plants **2:** 16012

Yamori W, Makino A, Shikanai T (2016) A physiological role of cyclic electron transport around photosystem I in sustaining photosynthesis under fluctuating light in rice. Sci Rep **6:** 20147

Yamori W, Shikanai T (2016) Physiological functions of cyclic electron transport around photosystem I in sustaining photosynthesis and plant growth. Annu Rev Plant Biol **67:** 81–106

Yamori W, Shikanai T, Makino A (2015) Photosystem I cyclic electron flow via chloroplast NADH dehydrogenase-like complex performs a physiological role for photosynthesis at low light. Sci Rep **5:** 13908